Laser-induced ultrafast spin dynamics in di-, tri- and tetranuclear nickel clusters, and the M process

D. Chaudhuri,[1,*] H. P. Xiang,[2,†] G. Lefkidis,[1] and W. Hübner[1]

[1]*Department of Physics and Research Center OPTIMAS, University of Kaiserslautern, P.O. Box 3049, 67653 Kaiserslautern, Germany*

[2]*Department of Physics and Astronomy, California State University Northridge, Northridge, California 91330-8268, USA*

(Received 31 July 2014; revised manuscript received 10 October 2014; published 4 December 2014)

In this manuscript we present an *ab initio* picture of ultrafast magneto-optical dynamics in clusters containing 2, 3, and 4 Ni atoms. The presence of the magnetic centers in the clusters renders our systems of choice highly interesting for studying ultrafast spin dynamics. Here we systematically study functional cooperativity by increasing both the number of active centers and the spin multiplicities included in our Hilbert space (singlets → triplets → quintets), and deriving several ultrafast, laser-driven, spin-manipulation scenarios. Our results indicate various cooperative effects like spin flip by the M process, and simultaneous spin flip and spin transfer, as well as reversible and irreversible demagnetization scenarios. As it turns out the functional cooperativity of the clusters strongly benefits from the delicate interplay of the spin multiplicity and the number of active centers.

DOI: 10.1103/PhysRevB.90.245113 PACS number(s): 71.15.−m, 75.60.Jk, 75.78.−n, 78.20.Ls

I. INTRODUCTION

Excitation by femtosecond laser pulses can induce a demagnetization in a nickel thin film on a subpicosecond time scale [1]. Since then there has been an intensive investigation on laser-induced magnetization dynamics [2–6]. Alteration of the anisotropy in the edge region of magnetized structures has significant effects on the magnetic properties that facilitate the design of a magnetic random access memory [7]. The effects of size and thickness of magnetic arrays on spin dynamics were also investigated [8]. Ultrafast dynamics is particularly important to fulfill the industrial demand for magnetic responses, which necessitates continuously decreasing sizes time scales. Scientific research in this field is particularly interesting since the microscopic mechanisms governing ultrafast magnetization are not yet fully understood. Thus the need for ultrafast magnetic dynamics is eminent both for magnetic recording and ultrafast information processing. Ultrafast electron-photon interaction can lead to subpicosecond dynamics [9]. Pump-probe experiments using the time-resolved (TR) magneto-optical Kerr effect (MOKE) [1], two-photon photoemission (TPPE) [3], and TR second harmonic generation (SHG) [2] have shown a very fast decay of magneto-optical signals. The physics behind the magnetization dynamics on femtosecond times scales is nontrivial and requires time-dependent, relativistic quantum mechanics and a many-body approach. Ultrafast dynamics in nickel and other transition metals (including extended systems) has been investigated both theoretically [10–14] and experimentally [15–19]. X-ray magnetic circular dichroism (XMCD) shows the importance of the spin-orbit interaction [18]. Other proposed models successfully describing aspects of ultrafast magnetization dynamics are (i) the superdiffusive spin transport mechanism [20], (ii) the Elliott-Yafet mechanism [21], (iii) relativistic quantum electrodynamic processes [22], (iv) the Landau-Lifshitz-Gilbert (LLG) equation [23], and (v) the Landau-Lifshitz-Bloch (LLB) micromagnetics schemes [24,25]. Extensive investigations on light-induced demagnetization in nickel have been performed previously [12,14,19,24]. Zhang *et al.* showed that the laser-induced ultrafast demagnetization is a cooperative effect of the internal exchange interaction, the spin-orbit coupling, and the external laser field [13].

In the Hartree-Fock (HF) theory the electron-electron interaction is handled in an averaged way. For a periodically extended system, integrals in real space over the infinitely extended system are replaced by integrals over the first Brillouin zone in reciprocal space (by summing over the function values over the integrand at a finite number of points in the Brillouin zone). In this manuscript we choose to treat the correlations of our systems in real space using state-of-the-art post-HF methods. We thus demonstrate the role of higher multiplets for spin dynamics and their relation to the specific level schemes of two-, three-, and four-magnetic-center clusters. We focus mainly on cooperativity effects and the laser-induced ultrafast spin dynamics.

Previous works exploited the well established Λ process on electronic states in order to realize spin-flip and spin-transfer scenarios in systems with two and three magnetic centers [26–28]. More specifically, the possibility of designing a prototypic magnetic-logic based on a realistic Ni_3Na_2 cluster in which the spins are manipulated in a targeted way (with proper use of a homogeneous external magnetic field and a laser pulse) was shown [27]. Up to now for obtaining functional cooperativity effects such as spin flip and spin transfer the number of active magnetic centers was restricted to *three*. However, by adding an extra magnetic center the explicit dependence on an external magnetic field can be removed. This motivates the study of *four*-magnetic-center structures [29,30]. The spin dynamics in systems with higher multiplicities is also *per se* of considerable interest. So far we restricted our calculations to *singlets* and *triplets*. Extending up to *quintets* provides more flexibility as it substantially enlarges the Hilbert space. It thus allows for additional functional-cooperativity effects and opens another avenue for designing logic elements for future spintronic devices.

Typically, two, three, and four magnetic center clusters come in three different environments: (a) bare, (b) surface

*chaudhuri@physik.uni-kl.de

†helenxianghp@gmail.com

supported, and (c) ligand stabilized. For (c) we refer to our previous work [31,32]. In the present manuscript we have situation (b) in mind, which we practically address by investigating case (a) for constrained geometries (dictated by the hypothetical surface). Electronic interactions of the magnetic clusters with a true substrate, similar to some previous investigated of ours for simpler substances [33], are neglected for simplicity.

We obtain various functional cooperative effects by three processes: (a) Λ process, (b) M process, and (c) nonlinear M process. A detailed introduction of these processes are as follows.

(a) Λ process. To achieve spin flip by this process, three states are required: two ground states with spin-up and spin-down configurations (initial and final states) and one intermediate spin-mixed state. The necessary spin mixing of the intermediate state can occur due to some magnetic mechanism (SOC and/or external magnetic field). This state is optically accessible from both the initial and final states. Generally the initial and the final states must have an energy difference of 0.1 meV. The energy difference between the ground states and the excited state must be larger than or equal to 0.5 eV so that the optical transitions between the states proceed rapidly. The name of the process originates from the resemblance with the Greek capital letter Λ. The entire process includes absorption of a photon of one helicity and the emission of another one of opposite helicity.

(b) M process. This process, which is similar to the Λ process, requires *five* states for a successful spin dynamics scenario. We name those states $|A\rangle$, $|B\rangle$, $|C\rangle$, $|D\rangle$, and $|E\rangle$ (see Fig. 3 in Sec. III A to compare) [34]. In all our processes, the initial state $|A\rangle$ and the final state $|E\rangle$ are quasidegenerate (in our successful scenarios although they do not stem from the ground state they lie energetically relatively low). The excited states $|B\rangle$ and $|D\rangle$ are also quasidegenerate. The transitions $|A\rangle \rightarrow |B\rangle$, and $|D\rangle \rightarrow |E\rangle$ are almost in resonance with the laser pulse. The middle intermediate state $|D\rangle$ lies energetically somewhat higher than states $|A\rangle$ and $|B\rangle$. The similarity of the whole process with the capital roman letter M justifies its nomenclature. The process involves the absorption of two photons of one helicity and the emission of two photons of the opposite helicity, thus effectively achieving the same functionality as the Λ process.

(c) Nonlinear M process. This process can be considered as an extension of the M process and requires seven states. Again, if we name them in sequence ($|A\rangle \rightarrow |B\rangle \rightarrow |C\rangle \rightarrow |D\rangle \rightarrow |E\rangle \rightarrow |F\rangle \rightarrow |G\rangle$), the initial state $|A\rangle$ and the final state $|G\rangle$ must be quasidegenerate and clearly lie above the ground state. The intermediate states $|B\rangle$ and $|F\rangle$ are also degenerate and lie energetically lower than $|A\rangle$ and $|G\rangle$. The intermediate states $|C\rangle$ and $|E\rangle$ are also quasidegenerate and lie energetically higher than $|A\rangle$ and $|G\rangle$. Finally the middle intermediate state $|D\rangle$ lies only slightly higher than the initial and the final states. This process involves not only four photons almost in resonance with the laser pulse (two absorptions of photons of the one helicity and two emissions of photons of the other helicity), but also the absorption and the emission of a photon with twice the energy of the laser pulse (transitions $|B\rangle \rightarrow |C\rangle$ and $|E\rangle \rightarrow |F\rangle$, respectively). This is the reason we call this process a nonlinear M process.

Our findings can be summarized as follows. (a) For an interatomic separation of 2.40 Å in Ni_2 we obtain a spin flip within 900 fs through an M process [35–37]. This process is an extension to the well-defined Λ process. (b) In Ni_3Na_2 we observe a simultaneous spin flip and transfer within 1500 fs for which appropriate level ordering is a prerequisite. To the best of our knowledge such a functionality has not been observed in extended systems so far. (c) If we include quintets states we observe a highly nonlinear M process where spin flips occur within 900 fs. (d) In the double dimer $(Ni_2)_2$ we find that we can manipulate the spin of each dimer separately. (e) Inclusion of higher multiplicities results in an irreversible global demagnetization process along with high fidelity global spin switching scenarios at a duration of 500 fs.

Throughout this manuscript we denote the multiplet states by ${}^{2s+1}|\Psi\rangle_{m_s}$, where $2s+1$ is the multiplicity (1, 2, or 3) and m_s the spin magnetic quantum number ($m_s = -s, -s+1, \ldots, s-1, s$). s is the spin azimuthal quantum number.

The manuscript is organized as follows. In Sec. II the theoretical background and some computational details are given. Section III presents our numerical results for the two-magnetic-center Ni_2 cluster (Sec. III A), the three-magnetic-center Ni_3Na_2 cluster (Sec. III B), and the double dimer, four-magnetic-center $(Ni_2)_2$ (Sec. III C).

II. THEORY AND METHODS

We intentionally calculate real systems instead of model systems to ensure that all crucial effects related to magnetic, transition-metal clusters are included on the level of first principles theory. Only in this way quantitative comparisons with experiments are possible (for an example, see [32]). For our theory both the accurate energies of the states and the exact wave functions are necessary (the latter to obtain the transition-matrix elements, e.g., the electric-dipole elements which govern the response of the system to any time-dependent electromagnetic field). We perform our calculations in three steps: (i) nonrelativistic high-level quantum-chemistry calculations, (ii) perturbative inclusion of spin-orbit coupling (SOC) and an external, static magnetic field, and (iii) computation of laser-induced global spin manipulation scenarios. A more detailed description of the steps follows.

(i) In the first step we solve the nonrelativistic model Hamiltonian of the magnetic system without any external field. The Hamiltonian reads

$$\hat{H}^{(0)} = -\frac{1}{2}\sum_{i=1}^{N_{\mathrm{el}}}\nabla^2 - \sum_{i=1}^{N_{\mathrm{el}}}\sum_{a=1}^{N_{\mathrm{at}}}\frac{Z_a}{|\mathbf{R}_a - \mathbf{r}_i|} + \sum_{i=1}^{N_{\mathrm{el}}}\sum_{j=1}^{N_{\mathrm{el}}}\frac{1}{|\mathbf{r}_i - \mathbf{r}_j|} + \sum_{a=1}^{N_{\mathrm{at}}}\sum_{b=1}^{N_{\mathrm{at}}}\frac{Z_a Z_b}{|\mathbf{R}_a - \mathbf{R}_b|}, \quad (1)$$

where N_{el} and N_{at} refer to the number of electrons and atoms, $\mathbf{r}_i$ and $\mathbf{r}_j$ refer to the position vectors of the electrons, $\mathbf{R}_a$ and $\mathbf{R}_b$ refer to the position vectors of the nuclei, and Z_a and Z_b are the charges of the nuclei. The third term on the right-hand side of the equation is of maximum importance as it gives rise to the electronic correlations.

We treat correlations with two distinct, yet closely related, coupled-cluster (CC) based methods as implemented in GAUSSIAN09 [38]. For the isolated Ni_2 cluster we calculate the ground state and the energetically lowest 30 excited states with the equation-of-motion coupled-cluster method with single and double excitations (EOM-CCSD) [39–44]. The calculation of the many-body excited states for Ni_3Na_2 is performed using the symmetry-adapted-cluster configuration-interaction (SAC-CI) method [45]. Here we first calculate the ground and 60 excited states consisting of 30 triplets and 30 singlets. Then we increase the complexity of the problem by including quintets in the excited states. We take into account, besides the ground state, 15 singlets, 15 triplets, and 15 quintets, thus including a total of 45 excited states. Lastly, for $(Ni_2)_2$ we calculate the lowest 40 excited states comprising 10 singlets, 15 triplets, and 15 quintets by the SAC-CI method. Of course, the inclusion of triplet and quintet states implies the inclusion of all substates within the state ($m_s = 1,0,-1$ for triplets, and $m_s = 2,1,0,-1,-2$ for quintets).

It is very important to emphasize the presence of two types of electronic excitations. (a) Virtual excitations from the single-determinantal reference state describe the many body nature of the state. (b) Real optical (laser) transitions between the many body states obtained in this way are mediated by dipole transition-matrix elements. Neither the excitations of type (a) nor the ones of type (b) are limited to single and double excitations in our calculations. A detailed elaboration of the excitations are as follows.

(a) Virtual excitations. The SAC-CI and EOM-CCSD approaches are versatile electronic-structure tools which can describe a variety of highly correlational wave functions [42]. With the use of CC methods it is possible to calculate many-body excited states with a single-reference formalism that handles both dynamic and static correlations. With respect to the latter, CC methods yield a much larger number of configurations than multireference methods such as the complete-active-space self-consistent-field (CAS-SCF) method. Despite this, the methods of our choice still cost us less computational overhead, because, unlike multireference methods, they deal with only one orthogonal set of molecular orbitals. This allows us to take full advantage of the Slater-Condon rules.

Unlike the simpler configuration interaction (CI), CC uses an exponential expansion of the excitation operators. Therefore these operators effectively appear not only isolated but also in combinations (leading among other to the famous size consistency of the method). Therefore, the sole characterization of single and double virtual excitation (which refers to the exponents only) is somewhat misleading, since several *simultaneous* single and double excitations are also accounted for (in other words many higher-order excitations are considered, the actual cutoff being their energy contribution) [42]. In this respect the methods used belong probably to the most advanced methods available today (by this we do not mean the theoretical investigation of methods but their applicability to actual systems).

(b) Optical transitions. For the propagation step we take into account *all* many-body states which can be addressed by our laser pulses (more than 130 many-body states). Therefore, in terms of virtual, one-electron excitations, one can easily trace back up to sextuple (and in some cases even higher-order) excitations. The many-body states, which are not included, are the ones which either cannot be addressed due to optical selection rules (as determined by their transition-matrix elements being five orders of magnitude weaker than the typical allowed ones), or are severely off-resonance (more than twice the energy of the laser pulse).

Both of the post HF methods we use (SAC-CI and EOM-CCSD) are size consistent [44,46–48], an intrinsic problem of simple CI, and yield eigenfunctions of the spin operator [44]. These closely related coupled-cluster methods describe both the *d-d* and charge-transfer transitions accurately. Thus both these quantum mechanical methods are very well suited to describe laser-induced femtosecond dynamics.

Previously we reported two kinds of dynamics, a phonon-driven one and an ultrafast laser-driven one. It is very important to mention that the "lattice" dynamics (in the molecule) and the electron relaxation channels are not distinguishable by the times scale as they are not different by orders of magnitude (as in extended systems). This is completely in line with our previous findings in Ni_3Na_2 where we obtain only a factor of 2 between the time scales of the lattice mediated (phonon-driven) and the electronic Λ processes [49]. Yet, they might take separate paths. In addition, we find a strong dependence of the many-body contributions on the bond lengths that results in a high target selectivity [50].

Moreover, potential transfer of the angular momentum to the nuclear system may play a potential role in a bare molecular system. This has already been discussed in the previous work for triangular Co_3 clusters but this goes beyond the scope of this paper [51].

It has already been shown that the presence of more determinants underlines the importance of correlations and enhances the chances of obtaining high-fidelity spin-dynamics scenarios [52]. This further justifies the use of coupled-cluster methods, which for our systems yield many-body states typically consisting of more than 1500 determinants.

In the SAC-CI the ground state is

$$|\Xi_g\rangle = \left(1 + \sum_I c_I S_I + \frac{1}{2}\sum_{I,J} c_I c_J S_I S_J + \cdots\right)|\Phi_0\rangle\,. \quad (2)$$

In the above equation $|\Phi_0\rangle$ is the Hartree-Fock many-body wave function, S_I, S_J are the symmetry-adapted excitation operators (single, double, or higher excitations), and c_I are the expansion coefficients. The single-excitation operators are

$$S_I = S_i^a = \frac{1}{\sqrt{2}}(a_{a\alpha}^\dagger a_{i\alpha} + a_{a\beta}^\dagger a_{i\beta}). \quad (3)$$

Operating on $|\Phi_0\rangle$ with S_I destroys an electron in the molecular orbital i and creates one in the molecular orbital a. This is extended to spin systems for the α (spin-up) and β (spin-down) electrons. Finally the excited states are determined via the cluster expansion of the SAC-CI wave function [53],

$$|\Xi_e\rangle = \left(\sum_K d_K R_K + \sum_{K,I} d_K c_I R_K S_I + \cdots\right)|\Phi_0\rangle$$

$$- \sum_K d_K S_{gK} |\Xi_g\rangle , \quad (4)$$

where $S_{gK} = \langle \Xi_g | R_K | \Xi_g \rangle$. The d_K are the normalization coefficients and R_K represents the excitation operator of the excited system.

The equation-of-motion (EOM) method is another quantum mechanical approach that calculates the energy differences between the states correctly. This is very important because these differences are directly connected to the experimentally observed spectra. The strength of the formalism lies in the clear choice of the reference and the target states. In CC methods the flexibility in choosing the reference state has enabled the EOM-CC model to treat electronically excited closed shell molecules and open-shell systems [43,44]. Correlations are treated separately in the reference and the excited states at a relatively low computational cost yielding compact representations and characterizations of the target states. Both EOM-CC and CI scale as N^6 with the system size N for single and double excitations. EOM-CC provides a balanced treatment of the dynamic and static correlations, thus allowing for an accurate calculation of the energy differences. The electronic wave functions within this scheme can be written as $|\Psi\rangle \approx \hat{R} e^{\hat{T}} |\Phi_0\rangle$. Obviously the choice of $|\Phi_0\rangle$ determines the Hartree-Fock vacuum, i.e., the separation of orbital space into occupied and virtual subspaces [44]. In the EOM method the excitation operators $\hat{R}$ and $\hat{T}$ commute as they act on the same reference state (they are also very similar to CI excitation operators). The targeted EOM states are found by diagonalizing the transformed Hamiltonian

$$\bar{H} = e^{-\hat{T}} H e^{\hat{T}}, \quad (5)$$

$$\bar{H} \hat{R} |\Phi_0\rangle = E \hat{R} |\Phi_0\rangle . \quad (6)$$

In EOM-CCSD, $\hat{T}$ and $\hat{R}$ are curtailed at single and double excitations, and the amplitudes $\hat{T}$ satisfy the CC equations for the reference state $|\Phi_0\rangle$

$$\hat{R} |\Phi_0\rangle = (\hat{R}_0 + \hat{R}_1 + \hat{R}_2 + \cdots) |\Phi_0\rangle$$
$$= \left(r_0 + \sum_{ia} r_i^a |\Phi_i^a\rangle + \frac{1}{4} \sum_{ijab} r_{ij}^{ab} |\Phi_{ij}^{ab}\rangle + \cdots \right) . \quad (7)$$

Here $|\Phi_i^a\rangle$ and $|\Phi_{ij}^{ab}\rangle$ refer to the single and double excitations, respectively. This method is size consistent, provided the amplitudes $\hat{T}$ satisfy the CC equations for $|\Phi_0\rangle$ and are truncated for a high level of excitations by the condition

$$\langle \Phi_\alpha | R_K | \Phi_0 \rangle = 0, \quad (8)$$

where Φ_α denotes the α-triply excited determinants in the case of single and double substitutions. In terms of computational capabilities, EOM-CCSD is numerically superior to other coupled-cluster methods and can very accurately describe dynamic correlations in the transformed Hamiltonian $\hat{H}$. EOM-CCSD is not explicitly developed to describe static correlations like other multireference methods; still it can deliver very accurate results on the price of a large number of single-reference determinants in the CI expansion (in our calculations a typical state consists of several hundreds of Slater determinants). Thus with different combinations of the excitation operators and the reference state $|\Phi_0\rangle$, various target states are obtained.

(ii) The second step is to solve the time-independent Hamiltonian in a static magnetic field $\mathbf{B}_{\text{stat}}$,

$$\hat{H}^{(1)} = \sum_{i=1}^{N_{\text{el}}} \frac{Z_a^{\text{eff}}}{2c^2 R_i^3} \hat{\mathbf{L}} \cdot \hat{\mathbf{S}} + \mu_L \hat{\mathbf{L}} \cdot \mathbf{B}_{\text{stat}} + \mu_S \hat{\mathbf{S}} \cdot \mathbf{B}_{\text{stat}}. \quad (9)$$

With the use of the one-electron Breit operator the SOC is calculated. Z_a^{eff} accounts for the two-electron integrals [54]. $\hat{\mathbf{L}}$ and $\hat{\mathbf{S}}$ are the orbital and spin angular momentum operators, μ_L and μ_S are their respective gyromagnetic ratios, and c is the speed of light. Relativistic effective nuclear charges Z_a^{eff} are used for the two-electron integrals of SOC. All the terms used in Eq. (9) describe intrinsic properties of the material. The necessity for the Zeeman splitting (second and third term in the above equation) arises among others from the need to (numerically) distinguish the different substates (different values of m_s) of the triplet and quintet states. Additionally it further lowers the symmetry of the system, thus creating more spin-mixed states, which can be used as intermediate states for our Λ and M processes.

(iii) In the third step the time-dependent contribution $\hat{H}^{(2)}(t)$ arising from the influence of the laser pulse can be written as

$$\hat{H}^{(2)}(t) = \hat{\mathbf{D}} \cdot \mathbf{E}_{\text{laser}}(t) + \hat{\mathbf{S}} \cdot \mathbf{B}_{\text{laser}}(t). \quad (10)$$

For the relativistic effects and the propagation we implement our own codes [55–60]. The laser parameters (angle of incidence, polarization, duration, and amplitude) are optimized with the use of our specially developed genetic algorithm [26]. The time-dependent calculation of the systems is performed within the interaction picture in the complete Hilbert space spanned by the eigenstates of Eq. (9) using an embedded fifth-order Runge-Kutta method and implementing the Cash-Karp adaptive-step control [61].

III. RESULTS

A. Nickel dimer (Ni_2)

The nickel atoms in Ni_2 are separated by 2.4 Å (Fig. 1). Section I presents the EOM-CCSD method used for the calculation of the excited states. We use the Los Alamos basis set with relativistic effective core potentials (Ni[8s5p5d/3s3p2d]) [62,63]. Pure spin states are prerequisites for spin dynamics. We solve the nonrelativistic Hamiltonian by the restricted Hartree-Fock (RHF) method. Generally, for our model of spin dynamics four levels are required: two states with spin-up and spin-down configurations (initial and final states) and two intermediate mixed-spin

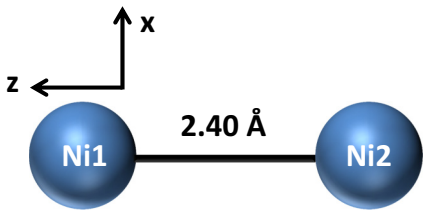

FIG. 1. (Color online) Structure of a nickel dimer Ni_2.

TABLE I. Optimized parameters of the laser pulse for the spin-switch and demagnetization scenarios for Ni_2, Ni_3Na_2, and $(Ni_2)_2$. Here, θ and ϕ denote the angles of incidence in spherical coordinates, respectively, and γ is the angle between the polarization of the light and the optical plane. FWHM is the full width at half maximum of the laser pulse.

Spin process (in Fig.)	Spin states	θ (deg)	ϕ (deg)	γ (deg)	Amplitude (a.u.)	Intensity ($J\,s^{-1}m^{-2}$)	FWHM (fs)	Energy (eV)
3	$^3\|4\rangle_{-1} \longrightarrow {}^3\|5\rangle_1$	27.21	143.20	3.16	0.30	2.35	500	1.49
10	$^5\|33\rangle_{-1} \longrightarrow {}^5\|35\rangle_1$	338.53	358.24	97.47	0.30	2.30	400	1.16
13	$^5\|9\rangle_{-2} \longrightarrow {}^5\|6\rangle_0$	79.45	207.97	289.61	0.29	2.16	350	1.90

excited states. The initial and final states are energetically close to the ground states and have an energy difference of 0.1 meV. The latter ones stem from spin-up and spin-down states which are coupled by a mechanism (SOC and/or a magnetic field). Of course at least one of the resulting intermediate states must be optically accessible from both initial and final states [64]. Without the application of the magnetic field the spin-up and spin-down states ($\langle S_z\rangle = 1$ and -1, respectively, in the absence of zero-field splitting) are degenerate; hence any linear combination is an eigenstate of the Hamiltonian. However, even a small magnetic field lifts these degeneracies (Zeeman effect) and make the states distinguishable. Since Ni_2 is a highly symmetric molecule we expect equal spin density on both atoms (the two unpaired electrons of a triplet will be equally distributed among both active centers). Correlations alone do not break the symmetry; therefore, a symmetry-breaking operator in the Hamiltonian is necessary. However, correlations can further enhance the effect, once the degeneracies are lifted. In principle, this can result in complete localization of the spins on one or the other—yet, it turns out that for our highly symmetric dimer this is not the case. For transition metal ions the interactions responsible for large splittings are the spin-orbit coupling (SOC) and the Zeeman effect (due to the external magnetic field). The lifting of the orbital degeneracies results in a nondegenerate ground state with zero orbital angular momentum. Our calculations show that the zero-field (ZF) splitting for the triplet ground state is 7.4 meV. A successful global spin switch scenario (M process) with a very high fidelity of $98 \pm 1\%$ is easily found. Similar calculations including quintets are not discussed here as they only slightly increase the spin densities on the atoms.

The optimized laser parameters for the successful spin-flip scenario by the M process are given in Table I. Previous results with respect to the tolerance of the effect regarding against spectral broadening and laser detuning also suggest experimental stability of the suggested scenarios [31].

Figures 2 and 3 present a complete spin reversal based on an M process, which involves many intermediate states with substantial transient occupations. The external magnetic field is applied along the z axis (which also means that in this case the sole spin-mixing mechanism is SOC and not, e.g., a Voigt geometry pertinent to semiconductors, in which the trion states remain unaffected [65]). A laser pulse of intensity 2.35 $Js^{-1}m^{-2}$ and energy 1.50 eV is used for the spin-flip process. The intermediate states are particularly important as they play a major role in the spin-flip scenarios. A transition between two states will proceed more rapidly the stronger the coupling between the states becomes. We know, as a rule of thumb, that for a successful Λ process the transition-matrix elements between the initial and the intermediate states (μ_1) must be of comparable magnitude to the transition-matrix elements between the final and intermediate states (μ_2), i.e., $|\mu_1| \approx |\mu_2|$ [10,66]. Whenever this condition is not met, spin flips and/or spin transfers are achieved via an M process [35–37]. In this context, we observe here another very important rule of thumb: the transition-matrix elements between the various states involved in the scenario (for a pictorial explanation refer to Fig. 2) must be related as $|\mu_1| \approx |\mu_4|$ and $|\mu_2| \approx |\mu_3|$. Note also that the energy differences $\Delta E_{|4\rangle\to|47\rangle} = 1.516$ eV and $\Delta E_{|5\rangle\to|48\rangle} = 1.513$ eV are almost in resonance with the laser pulse (1.5 eV). Unlike Λ processes, here we have a sequence of four optical transitions $|4\rangle \longrightarrow |47\rangle \longrightarrow (|16\rangle + |17\rangle) \longrightarrow |48\rangle \longrightarrow |5\rangle$; see also Fig. 3.

At this point we can say as a rule of thumb that if a Λ process is not possible (i.e., due to the lack of addressable intermediate states) often a spin-flip scenario can still successfully occur through an M process. The time, however, is expected to be longer, since it includes more intermediate states and involves four rather than two photons. The symmetry of the M process is reflected in the dynamic pathway of the z component of

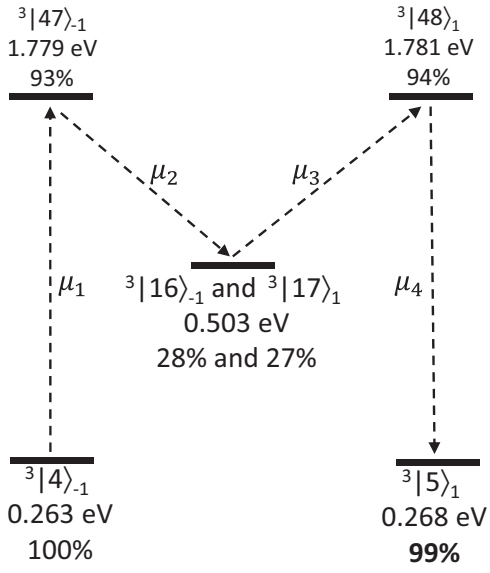

FIG. 2. Schematic of the spin-flipping M process in Ni_2. $\mu_n (n = 1,2,3,4)$ are the transition-matrix elements. Depicted are the involved states and their energies (in eV), as well as their maximal transient occupation during the whole process. The occupation of the final state $^3|5\rangle_1$ (99%) is printed in bold, because it is also the fidelity of the whole process. States $^3|16\rangle_{-1}$ and $^3|17\rangle_1$ are quasidegenerate. Compare also with Fig. 3.

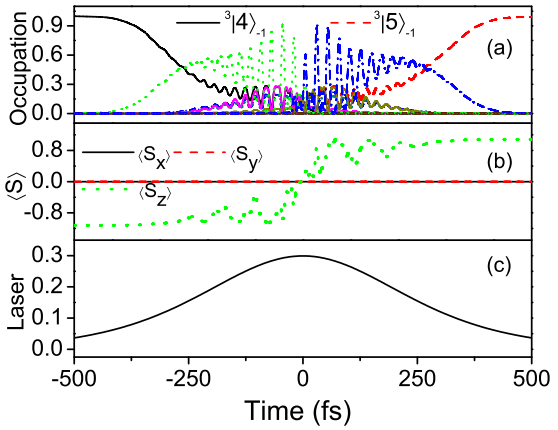

FIG. 3. (Color online) Global spin-flip scenario in Ni_2. Top: time-resolved occupations of the initial (solid black line), final (dashed red line), and some of the intermediate states. Middle: time-resolved x (solid black line), y (dashed red line), and z (dotted green line) component of the spin. Bottom: the envelope of the laser pulse.

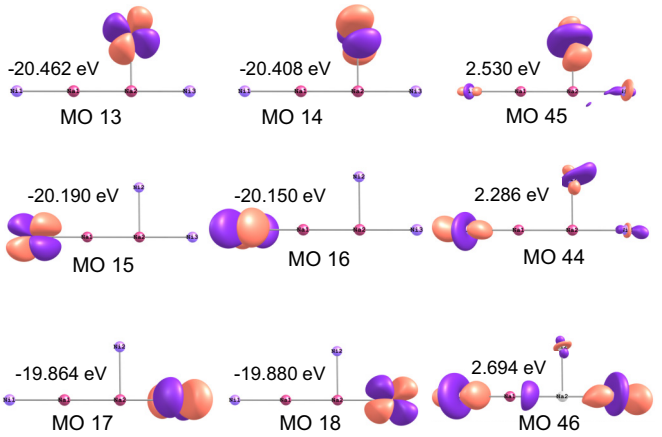

FIG. 5. (Color online) Some of the strongly localized, single-electron, d-character molecular orbitals in the three-magnetic-center Ni_3Na_2 cluster. The multiplicity of the cluster for the HF step is triplet. The isosurfaces of the molecular orbitals are dark violet and orange for positive and negative values, respectively.

the spin angular momentum. Here we report the possibility of global spin flip within 900 fs (Fig. 3).

B. Three-magnetic-center Ni_3Na_2 cluster

The structure used for the calculations is shown in Fig. 4. Figure 5 shows some of the most important d-character molecular orbitals (MO) resulting from the HF calculation. Although our highly correlated, post-HF wave functions cannot be described by such simplified pictures, the latter ones can still be useful to qualitatively pinpoint the main, virtual one-electron excitations included in the many-body wave functions (which we use for all subsequent dynamics calculations) and to give some insight into the spin localization of the different many-body electronic states. As examples we mention the many-body quintet state $^5|12\rangle_1$ with the main virtual, one-electron excitation from MO 13 (with a strong d_{yz} character localized on Ni2) to MO 45 (with a strong d_{y^2} character localized on Ni2) and a CI coefficient of 0.7768, the state $^5|33\rangle_1$ with the main virtual, one-electron excitation from MO 15 (with a strong d_{xy} character localized on Ni1) to MO 44 (with a strong d_{x^2} character localized on Ni2) and a CI coefficient of 0.5961, and finally the many-body quintet state $^5|18\rangle_1$ with the main virtual, one-electron excitation from MO 18 (with a strong d_{xz} character localized on Ni3) to MO 46 (with a strong d_{x^2} character localized almost equally on Ni1 and Ni3) and a CI coefficient of 0.6322. All three states play an important role for spin-manipulation scenarios (see also Table III). So evidently the localization of the MOs qualitatively reflects on the localization of the many-body states, the transition-matrix elements, and the optical selection rules in the system.

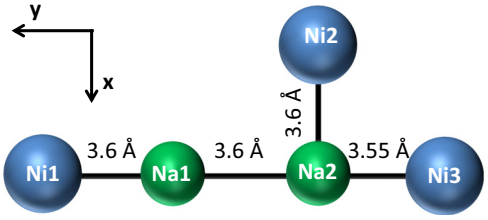

FIG. 4. (Color online) Geometrical structure of the three-magnetic-center Ni_3Na_2 cluster. The numbers show the interatomic distances in Å.

1. *Singlets and triplets in Ni_3Na_2*

The present section deals with the Λ process for triplets while we will reconsider the M process [35–37] for the quintets subspace in the next subsection. Xiang *et al.* reported the effects of lattice distortions on spin dynamics by varying the interatomic distance [27,49,57]. The presence of magnetic phases helped to distinguish two kinds of spin dynamics (slow phonon driven and ultrafast laser driven). This structure gives an insight to the functionality of simultaneous spin flip and transfer (spin flip transfer) with triplet excited states. The presence of a specific level ordering is a prerequisite for this functionality (see Table II). This particular level ordering, which we call interlocking, means that two triplet states are energetically so close that the lowest substate of the upper triplet state has lower energy than the highest substate of the lower triplet state (same as interlocking the fingers of both hands). Interlocking leads to intermediate states stemming from *both* quasidegenerate triplet states, thus opening a channel for both spin switch (due to mixing of

TABLE II. Presence of level ordering or interlocking of triplet excited states in Ni_3Na_2.

State	Energy (eV)	⟨S⟩	Direction	Localization
10	0.1943	1.866	→	Ni3
9	0.1943	1.824	↗	Ni2
8	0.1924	1.870	←	Ni3
7	0.1921	1.826	↙	Ni2

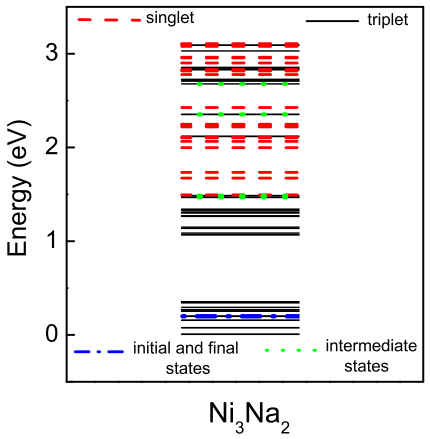

FIG. 6. (Color online) Energy levels of the excited states for Ni_3Na_2 without SOC. The states marked in blue (dash-dotted line) are the initial and final states from the simultaneous spin flip and transfer scenarios and the green (dotted lines) indicate the intermediate states.

spin-up and spin-down states) and spin transfer (if the two triplets exhibit different spin-density localizations), as is the case with states $|7\rangle$ to $|10\rangle$.

As can be deduced from Table II, states $|7\rangle$ and $|9\rangle$ occur from the spectral splitting of the same triplet state due to the Zeeman effect and SOC, and the spin density of both is localized on Ni2. $|8\rangle$ and $|10\rangle$ are also substates of one triplet state that are split by the Zeeman effect and SOC. This time with the spin density is localized on Ni3. Another important aspect is the direction of the spin (along the $\pm x$ direction for $|7\rangle$ and $|9\rangle$, but along the $\pm xy$ direction for $|8\rangle$ and $|10\rangle$). A successful transfer of spins between the interlocked states, i.e., $|7\rangle \longrightarrow |10\rangle$ and $|8\rangle \longrightarrow |9\rangle$ promotes a functional cooperativity effect, i.e., simultaneous spin flip and spin transfer (spin flip transfer) within 1500 fs (Fig. 8). The feasibility of this effect largely depends on the energy difference and the coupling between the interlocked states (Fig. 6).

The results for the spin manipulation scenarios using triplet states are summarized in the upper half of Table III. Regarding local spin flips we see that on Ni3, we find the process achieves a very high fidelity of 91% ($|8\rangle \longrightarrow |10\rangle$) with a laser-pulse intensity of 1.66 $J\,s^{-1}m^{-2}$, whereas on Ni2 it only reaches 75% ($|7\rangle \longrightarrow |9\rangle$) despite the almost four times more intense laser pulse (6.53 $J\,s^{-1}m^{-2}$). In both cases the spin flip is concluded within 600 fs. In the spin-transfer scenario we find two scenarios ($|7\rangle \longrightarrow |8\rangle$ and $|9\rangle \longrightarrow |10\rangle$), both of which reach a fidelity of 87% and finish within 300 fs. The laser intensities for the two processes, however, are quite different: 2.37 $J\,s^{-1}m^{-2}$ for the $|7\rangle \longrightarrow |8\rangle$ transition and 1.89 $J\,s^{-1}m^{-2}$ for $|9\rangle \longrightarrow |10\rangle$ transition, respectively.

TABLE III. Some functionalities in Ni_3Na_2, divided in triplets (up) and quintets (down) subspaces.

State	Fidelity	Localization	Functionality
${}^3\|7\rangle_{-1} \longrightarrow {}^3\|9\rangle_1$	75%	Ni2	Spin flip
${}^3\|8\rangle_{-1} \longrightarrow {}^3\|10\rangle_1$	91%	Ni3	Spin flip
${}^3\|7\rangle_{-1} \longrightarrow {}^3\|8\rangle_1$	87%	Ni2 → Ni3	Spin transfer
${}^3\|9\rangle_1 \longrightarrow {}^3\|10\rangle_1$	87%	Ni3 → Ni2	Spin transfer
${}^3\|7\rangle_{-1} \longrightarrow {}^3\|10\rangle_1$	72%	Ni2 → Ni3	Spin-flip transfer
${}^3\|8\rangle_{-1} \longrightarrow {}^3\|9\rangle_1$	70%	Ni3 → Ni2	Spin-flip transfer
${}^5\|33\rangle_{-1} \longrightarrow {}^5\|35\rangle_1$	93%	Ni1	Spin flip
${}^5\|12\rangle_{-1} \longrightarrow {}^5\|15\rangle_1$	97%	Ni2	Spin flip
${}^5\|18\rangle_{-1} \longrightarrow {}^5\|19\rangle_1$	87%	Ni3	Spin flip
${}^5\|16\rangle_{-2} \longrightarrow {}^5\|18\rangle_0$	89%	Ni2	Demagnetization
${}^5\|11\rangle_{-2} \longrightarrow {}^5\|14\rangle_0$	81%	Ni3	Demagnetization

The most challenging scenario that demands the highest degree of cooperativity of the magnetic centers is the spin-flip-transfer scenario $|7\rangle \longrightarrow |10\rangle$ with a fidelity of 72%. The process requires 1500 fs, i.e., more than twice the time required for the simple flip, and four times the time of the transfer scenarios, and needs a ten times more intense laser pulse (26.3 $J\,s^{-1}m^{-2}$). A laser pulse of the same intensity (but slightly different geometry of incidence) can also trigger the transition $|8\rangle \longrightarrow |9\rangle$, however with a somewhat lower fidelity (70%). The states involved in the process (before SOC splitting) are shown in Fig. 6, while Fig. 7 shows the time evolution of the populations of involved states and the expectation value of $\langle \mathbf{S} \rangle$, as well as the envelope of the laser pulse. Figure 8 schematically summarizes all spin-manipulation scenarios (spin flip, spin transfer, and spin flip transfer) found on Ni_3Na_2. What is definitely noteworthy is that *all* twelve transitions within the Hilbert subspace spanned by the four interlocked states are possible.

2. *Triplets and quintets in Ni_3Na_2*

Quintets substantially increase the complexity of the problem, but at the same time they open an avenue for the emergence of more functional cooperativity effects like local spin-flip and local demagnetization scenarios. This can be easily understood by analyzing the total-angular momentum conservation during a Λ process. The process includes the

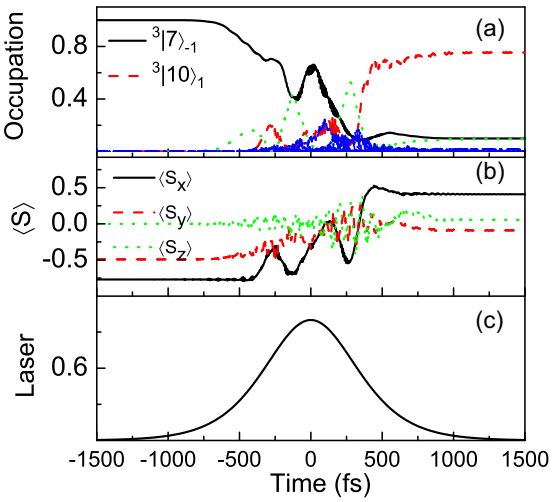

FIG. 7. (Color online) Simultaneous spin flip and transfer in Ni_3Na_2. Top: time-resolved occupations of the initial (solid black line), final (dashed red line), and some of the intermediate states. Middle: time-resolved x (solid black line), y (dashed red line), and z (dotted green line) component of the spin. Bottom: the envelope of the laser pulse.

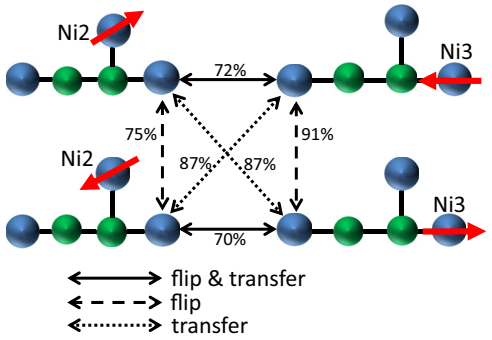

FIG. 8. (Color online) Sketch map showing various functionalities obtained for the structure with singlets and triplets in the excited states. The directions of the arrows on the magnetic centers represent the direction of the spins. From the pictorial representation it is clear that simultaneous spin flip and transfer can be achieved between Ni2 and Ni3 with modest fidelity and local spin flips and transfers can be achieved with high fidelities.

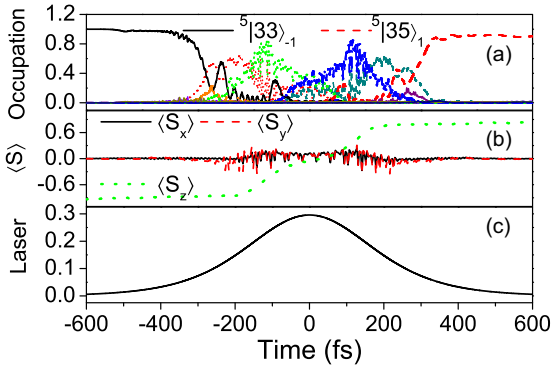

FIG. 9. (Color online) Global spin-flip scenario using quintets in Ni_3Na_2. Top: time-resolved occupations of the initial (solid black line), final (dashed red line), and some of the intermediate states. Middle: time-resolved x (solid black line), y (dashed red line), and z (dotted green line) component of the spin. Bottom: the envelope of the laser pulse. The initial state is $^5|33\rangle_{-1}$ and the final state is $^5|35\rangle_1$. The reached fidelity is 93%. See also Table III.

absorption of a boson (photon) of one helicity and the emission of another boson (photon) of the opposite helicity, leading to a net angular-momentum change of $\Delta J = \pm 2$ for the system [6]. If we restrict ourselves to singlet and triplet states only, there are only two possible transitions obeying this selection rule, namely $^3|\Psi\rangle_1 \longrightarrow {}^3|\Psi\rangle_{-1}$ and $^3|\Psi\rangle_{-1} \longrightarrow {}^3|\Psi\rangle_1$. Hence only spin flip is possible. (Of course this selection rule can be overcome by proper tilting of the magnetic field and the laser pulse, but then the transition requires longer times, as the projection of the transition-matrix elements on the new easy axis and propagation direction are smaller.) In other words, a demagnetization scenario of the type $^3|\Psi\rangle_{\pm 1} \longrightarrow {}^3|\Psi\rangle_0$ is not favored. Please keep in mind that in order to numerically differentiate between the substates of a triplet state ($\langle S_z\rangle = 1$, 0, and -1), we always need a minimal Zeeman splitting. Also note that not even an M process can overcome this difficulty, since there is always an even number of photons involved. This situation changes upon inclusion of the quintet states, for which a demagnetization process obeying the same selection rule is possible, namely the process $^5|\Psi\rangle_{\pm 2} \longrightarrow {}^5|\Psi\rangle_0$. The spin flips still exist ($^5|\Psi\rangle_1 \longrightarrow {}^5|\Psi\rangle_{-1}$ and $^5|\Psi\rangle_{-1} \longrightarrow {}^5|\Psi\rangle_1$). This is the remarkable benefit of such quintet states, where both local spin-flip and local demagnetization scenarios can be realized (indeed occurs for Ni_3Na_2).

An interesting characteristic of three-magnetic-center structures is that the electrons of a quintet state (four unpaired electrons) cannot be equally divided among the three centers (as is the case, e.g., for triplets and the dimer Ni_2). This incommensurability strengthens the spin-density localization and obviously enhances the fidelity of the processes. On Ni2 we derive local spin flip with the highest fidelity of up to 97% ($^5|12\rangle_{-1} \longrightarrow {}^5|15\rangle_1$), on Ni1 with a fidelity of 93% ($^5|33\rangle_{-1} \longrightarrow {}^5|35\rangle_1$), and the lowest fidelity, which still reaches 87%, on Ni3 ($^5|18\rangle_{-1} \longrightarrow {}^5|19\rangle_1$). Local demagnetization scenarios such as $^5|16\rangle_{-2} \longrightarrow {}^5|18\rangle_0$ and $^5|11\rangle_{-2} \longrightarrow {}^5|14\rangle_0$ are found on Ni2 and Ni3 with respective fidelities of 89% and 81%. For all the above mentioned scenarios the applied magnetic field is 2.35 T along the z direction. Note that in order to reduce the computational time, for the demagnetization scenarios the laser pulse was optimized only within the quintet Hilbert subspace, while the spin-flip scenarios were optimized within the quintet-triplet Hilbert subspace. The lower half of Table III summarizes the various functionalities found.

As it turns out, some of the spin-flip scenarios within the quintet subspace are much more complex than simple Λ processes. Figure 9 schematically depicts such a scenario on Ni1 (the other two processes of Table III are the usual Λ processes), for which a long chain of electronic transitions is necessary, i.e., $|33\rangle \longrightarrow |2\rangle \longrightarrow |72\rangle \longrightarrow (|47\rangle + |49\rangle) \longrightarrow |74\rangle \longrightarrow |4\rangle \longrightarrow |35\rangle$. The symmetry is also reflected in the time-resolved spin angular-momentum components. A simplified pictorial representation of the nonlinear population transfer pathway is shown in Fig. 10 and it can be mapped to the M process. Unlike the M process described in Sec. III this process is highly nonlinear. The electric-dipole transition-matrix elements (μ) between the states are related as $|\mu_1| \approx$

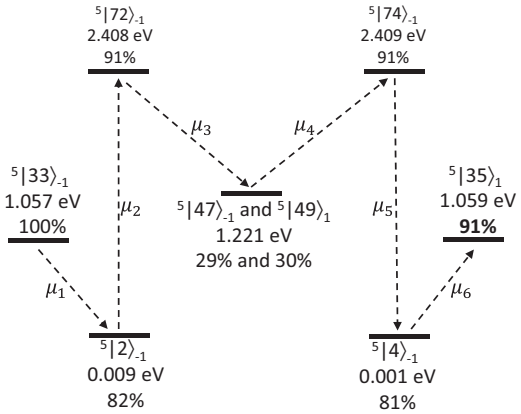

FIG. 10. Schematic representation of a nonlinear M process and simplified pictorial representation of the population transfer process. Indicated are the involved states, their energies, and their maximum transient occupations during the whole process. The energy of the laser pulse is 1.163 eV. The occupation of the final state $^5|35\rangle_1$ (91%) is printed in bold because it is also the fidelity of the whole process.

$|\mu_6|$, $|\mu_2| \approx |\mu_5|$, and $|\mu_3| \approx |\mu_4|$. This rule of thumb must be satisfied to achieve a successful scenario with maximum fidelity. The energy of the applied laser pulse is 1.163 eV. Upon careful inspection of all the transitions between the states we detect two two-photon transitions (off-resonant transitions, i.e., $|2\rangle \rightarrow |72\rangle$ and $|74\rangle \rightarrow |4\rangle$) with transition energies $\Delta E_{|2\rangle\rightarrow|72\rangle} = 2.339$ eV and $\Delta E_{|74\rangle\rightarrow|4\rangle} = 2.4008$ eV, respectively (almost twice the energy of the laser pulse), that makes the process highly nonlinear.

Concluding this section we summarize our findings. (a) For triplet excited states spin flip (on Ni2 and Ni3) and spin transfer (Ni2 $\longleftrightarrow$ Ni3) are achieved within 600 fs and 300 fs, respectively. In addition we report a combined functionality, i.e., simultaneous spin flip and spin transfer (spin flip transfer), which necessitates a much more intense laser pulse and longer time scales (1500 fs). (b) The presence of a specific electronic-level ordering (interlocking) is a prerequisite for this functionality. Including quintets in the excited states we find a highly nonlinear process which can be loosely compared with the M process found in Ni_2. Like its counterpart (M process), the transition time for this nonlinear process is 900 fs. (c) Besides local spin-flip scenarios we report the presence of local demagnetization scenarios on Ni2 and Ni3 within 600 fs by including quintet states. The cooperative effects reported here are solely based on first principles. (d) Considering the fitness of the attained functional cooperative effects we infer that the M process is equally efficient as compared to the Λ process. The price to pay, however, is that the total completion time is longer than a simple Λ process since the former consists of more electronic transitions.

C. Double nickel dimer $(Ni_2)_2$

In this section we discuss the system of two interacting, yet distinguishable nickel dimers separated by a distance of 6–7 Å. The interatomic distance of each dimer is 2.15 Å. The motivation behind this is twofold. First, we want to investigate the effect of the presence of a fourth magnetic center and, secondly, we want to study the possibility of using the spin of the one dimer as a source of an external magnetic field to control the spin on the other dimer (as has been proposed for magnetic logic elements [27]). Obviously, such an interaction cannot be described classically; a simple classical-electrodynamics calculations yields a necessary intermolecular distance between the two dimer in the order of 0.3 Å, which cannot be true. Therefore, a fully quantum mechanical description of the overall system is needed. As it turns out, a distance of 6–7 Å between the two dimers fulfills the purpose of the present research. At this distance both dimers still retain much of their identities, but interact with each other quantum mechanically. Larger separation results in two identical, very weakly interacting dimers. It is known that a sudden reversal in the direction of the external magnetic field can affect the magnetization of a ferromagnetically coupled chain adsorbed on the surface. This can be described as a sudden change in the direction of the magnetic moments within the chain. The sudden reversal promotes the chain to an excited state which eventually relaxes towards the ground state by interacting with the substrate electrons. This switching mechanism can be classified as global in nature [67].

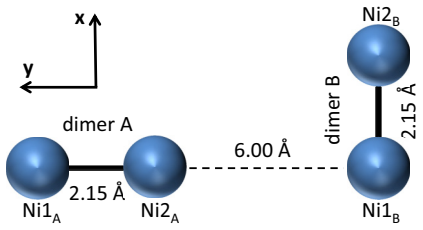

FIG. 11. (Color online) Relative orientation of the two dimers. The interatomic distance of both dimers A and B is 2.15 Å.

We again use the SAC-CI [45] package in the GAUSSIAN09 [38] for the calculation of the excited states. The Los Alamos basis set with relativistic effective core potentials (Ni[$8s5p5d/3s3p2d$]) is also used [62,63]. The orientation shown in Fig. 11 is chosen in order to lower the symmetry, which will influence the spin density distributions on both dimers. We also include quintets in the excited states, which we expect to open different spin-manipulation channels than the triplets. The reason is that our structure consists of four magnetic centers and is therefore commensurate with the number of unpaired electrons in a quintet state. This, in turn, results often in an equidistribution of the spin density in quintet states (clearly this is not the case for triplets with only two unpaired electrons). In other words we expect quintet states to give rise to global, equidistributed spin-flip scenarios, and triplet states to spin-flip scenarios localized on one dimer only. In more detail the spin-adapted configurations for the quintets are

$$^5|\psi\rangle_2 = \left|\psi^{ab}_{\bar{i}\bar{j}}\right\rangle, \tag{11}$$

$$^5|\psi\rangle_1 = \frac{1}{2}\left(\left|\psi^{\bar{a}b}_{\bar{i}\bar{j}}\right\rangle + \left|\psi^{a\bar{b}}_{\bar{i}\bar{j}}\right\rangle - \left|\psi^{ab}_{i\bar{j}}\right\rangle - \left|\psi^{ab}_{\bar{i}j}\right\rangle\right), \tag{12}$$

$$^5|\psi\rangle_0 = \frac{1}{\sqrt{6}}\left(\left|\psi^{\bar{a}\bar{b}}_{\bar{i}\bar{j}}\right\rangle + \left|\psi^{ab}_{ij}\right\rangle - \left|\psi^{a\bar{b}}_{i\bar{j}}\right\rangle - \left|\psi^{a\bar{b}}_{\bar{i}j}\right\rangle - \left|\psi^{\bar{a}b}_{i\bar{j}}\right\rangle - \left|\psi^{\bar{a}b}_{\bar{i}j}\right\rangle\right), \tag{13}$$

$$^5|\psi\rangle_{-1} = \frac{1}{2}\left(\left|\psi^{a\bar{b}}_{ij}\right\rangle + \left|\psi^{\bar{a}b}_{ij}\right\rangle - \left|\psi^{\bar{a}\bar{b}}_{\bar{i}j}\right\rangle - \left|\psi^{\bar{a}\bar{b}}_{i\bar{j}}\right\rangle\right), \tag{14}$$

$$^5|\psi\rangle_{-2} = \left|\psi^{\bar{a}\bar{b}}_{ij}\right\rangle. \tag{15}$$

The above equations describe virtual double excitations from the HF configuration where i and j are the occupied molecular orbitals, and a and b are unoccupied molecular orbitals. An orbital without overbar is an α (spin-up) MO, while an overbar indicates a β (spin-down) MO. As an example the Slater determinant $|\psi^{ab}_{\bar{i}\bar{j}}\rangle$ results from the HF Slater configuration with two virtual, one-electron excitations, namely two spin-flipping excitations (from β to α) from MOs i and j to MOs a and b. In general, at least two electrons must be virtually excited from the closed-shell HF configuration in order to get four unpaired electrons and this makes the quintets more correlated than triplets (which can be built with single excitations).

Table IV shows the spin density localization of the interesting states (with a magnetic field applied along the z direction), which indeed exhibits the expected behavior, i.e., equidistribution for quintets, and localization on one dimer

TABLE IV. Spin localizations for some of the triplets (up) and quintet (down) states of $(Ni_2)_2$.

State	$(Ni1)_A$	$(Ni2)_A$	$(Ni1)_B$	$(Ni2)_B$	Energy (eV)	$\langle S_z \rangle$
$^3\|15\rangle_1$	0.000	0.000	1.000	1.000	0.162	0.713
$^3\|13\rangle_{-1}$	−0.000	−0.000	−1.000	−1.000	0.159	−0.714
$^3\|2\rangle_1$	0.985	0.986	0.005	0.015	0.002	0.837
$^3\|1\rangle_{-1}$	−0.985	−0.986	−0.005	−0.015	0.000	−0.837
$^5\|10\rangle_2$	0.995	0.994	1.000	1.012	0.114	1.305
$^5\|9\rangle_{-2}$	−0.995	−0.994	−1.000	−1.012	0.112	1.305
$^5\|8\rangle_1$	0.498	0.494	0.501	0.507	0.112	0.221
$^5\|7\rangle_1$	−0.498	−0.494	−0.501	−0.507	0.107	−0.221
$^5\|6\rangle_0$	0.000	0.000	0.000	0.012	0.107	0.155
$^5\|4\rangle_1$	0.497	0.497	0.515	0.505	0.001	0.705
$^5\|2\rangle_{-1}$	−0.497	−0.497	−0.515	−0.505	0.000	0.706

only for triplets. In total we can derive the following scenarios on $(Ni_2)_2$: (i) local spin flip on dimer A using triplets, (ii) local spin flip on dimer B using triplets, (iii) global spin flip using quintets, (iv) global demagnetization using quintets, and (v) global, partial demagnetization using quintets. The scenarios are summarized in Table V.

Several characteristics are observed. One is the general global character of the quintet scenarios with respect to the more local character of the triplet scenarios. As mentioned above, this can be attributed to the number of unpaired electrons and the degree of correlations. Another important one is that for a given quintet state, it is possible to cycle through all the substates [see Fig. 12(a)]. Note, however, that not all transitions are achieved; only transitions with $|\Delta J| \leqslant 2$ are possible. To understand this one has to keep in mind the already mentioned $\Delta J = \pm 2$ selection rule that can be relaxed if the magnetic field and the propagation direction of the laser pulse are properly tilted. However, Λ processes only induce up to two-photon processes, which is why even the relaxation of the above selection rule does not permit transitions with $|\Delta J| > 2$. The transitions with the largest fidelity are within the quintet subspace [cases (iii), (iv), and (v)] summarized in Fig. 12(a). Within the triplet subspace only the usual Λ processes are achieved. The localization of the states (either dimer A or dimer B) reflects our original intention, i.e., that the two dimers are, to a certain extent, different entities and can be separately manipulated. Thus we report one of the important findings that with proper choice of multiplicity, the supermolecule or the dimer can be manipulated.

TABLE V. Some functionalities in $(Ni_2)_2$ divided in triplets (up) and quintets (down) subspaces. See also with Fig. 12.

States	Fidelity	Localization	Functionality
$^3\|1\rangle_{-1} \longrightarrow {}^3\|2\rangle_1$	91%	$(Ni_2)_A$	Spin flip
$^3\|13\rangle_{-1} \longrightarrow {}^3\|15\rangle_1$	89%	$(Ni_2)_B$	Spin flip
$^5\|2\rangle_{-1} \longrightarrow {}^5\|4\rangle_1$	91%	None	Global spin flip
$^5\|9\rangle_{-2} \longrightarrow {}^5\|6\rangle_0$	96%	None	Global demag.
$^5\|10\rangle_2 \longrightarrow {}^5\|6\rangle_0$	95%	None	Global demag.
$^5\|10\rangle_2 \longrightarrow {}^5\|8\rangle_1$	88%	None	Partial demag.
$^5\|9\rangle_{-2} \longrightarrow {}^5\|7\rangle_{-1}$	86%	None	Partial demag.

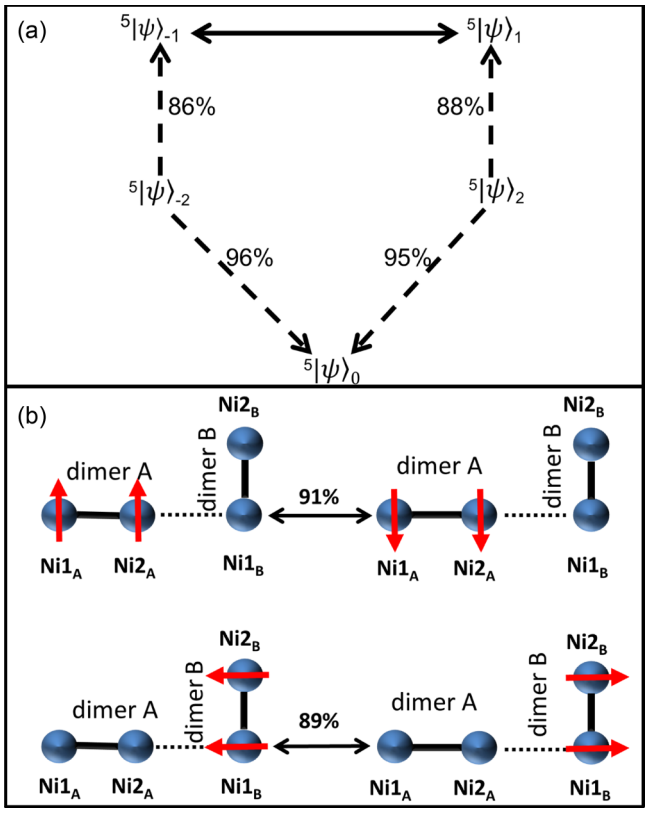

FIG. 12. (Color online) Schematic of all spin-manipulation scenarios in $(Ni_2)_2$. (a) Scenarios for quintets. The bidirectional solid arrow represents a reversible process with fidelities; the unidirectional dashed arrows represent irreversible processes. All scenarios are global (the spin density is equidistributed on all Ni atoms). (b) Scenarios for triplets. The bidirectional solid arrows represent reversible processes. The numbers are the fidelities of the process. The red arrows on the atoms show the spin localization and direction. See also Table V.

Our final observation, which is also unique to $(Ni_2)_2$ and takes place only within the quintet subspace, is that we observe both reversible and irreversible processes. The vast majority of our spin-manipulation scenarios are reversible in the sense that the same optimized laser pulse induces both the forward and the backward transition with high fidelity (e.g., both $^3|1\rangle_{-1} \longrightarrow {}^3|2\rangle_1$ and $^3|2\rangle_1 \longrightarrow {}^3|1\rangle_{-1}$). Of course strictly mathematically speaking all our propagations are reversible, since we perform only unitary transformations of the wave function under the influence of the laser pulse, and any relaxations in this coherent regime are neglected. However, the reverse scenario is expected to have exactly the same fidelity, only if we start from the exact final state of the propagation. This state may slightly differ from the targeted one. In performing the transition $^5|10\rangle_2 \longrightarrow {}^5|6\rangle_0$ (Table V) we end up with a state which consists of only 95% of the desired state. When performing the process in the opposite direction we start from 100% state $^5|6\rangle_0$. These small admixtures are sometimes enough to completely alter the outcome of the two directions, and can be the result of relaxation *after* the application of the laser pulse. In fact this mechanism has already been exploited to create the ERASE functionality [58], which theoretically allows the targeted preparation of a specific substate (which

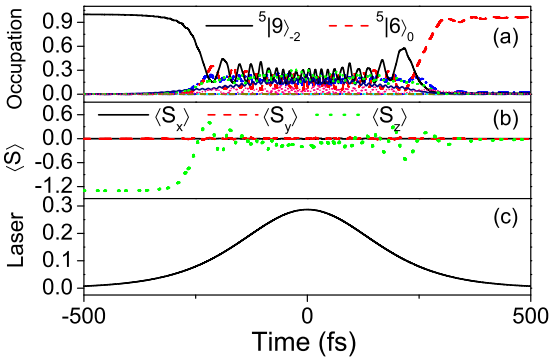

FIG. 13. (Color online) High-fidelity forward $^5|9\rangle_{-2} \longrightarrow {}^5|6\rangle_0$ demagnetization process in $(Ni_2)_2$. Top: time-resolved occupations of the initial (solid black line), final (dashed red line), and some of the intermediate states. Middle: time-resolved x (solid black line), y (dashed red line), and z (dotted green line) component of the spin. Bottom: the envelope of the laser pulse. See also Table V.

can never occur in a thermalized system). So while the demagnetization transition $^5|9\rangle_{-2} \longrightarrow {}^5|6\rangle_0$ reaches a fidelity of 96% (Fig. 13), the opposite transition $^5|6\rangle_0 \longrightarrow {}^5|9\rangle_{-2}$ is only half as effective and merely reaches 55% fidelity (Fig. 14). There are probably two reasons for this. First, quintet states are generally more correlated, thus making all processes more sensitive to all kinds of perturbations of the initial conditions. Secondly, which seems more important here, is that within a quintet state, the $^5|\Psi\rangle_0$ substate consists of six times more Slater determinants than the $^5|\Psi\rangle_{\pm 2}$ substates. Therefore, the already high dependence on the initial conditions becomes even more imbalanced at the two ends of the process. This hypothesis is further substantiated when investigating the reversibility of the partial demagnetization processes. The transition $^5|10\rangle_2 \longrightarrow {}^5|8\rangle_1$ reaches 88%, while the opposite direction goes only up to 83%. In this case the difference is smaller because the difference in the number of Slater determinants in the CI expansions of the two is smaller ($^5|\Psi\rangle_1$ has 1.5 times as many determinants as $^5|\Psi\rangle_2$).

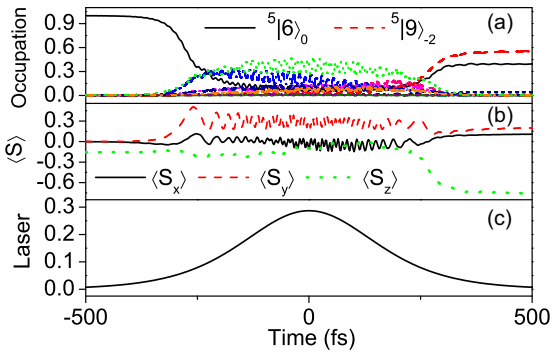

FIG. 14. (Color online) Backward propagation of the irreversible demagnetization in $(Ni_2)_2$. The scenario depicted is $^5|6\rangle_0 \longrightarrow {}^5|9\rangle_{-2}$. Top: time-resolved occupations of the initial (solid black line), final (dashed red line), and some of the intermediate states. Middle: time-resolved x (solid black line), y (dashed red line), and z (dotted green line) component of the spin. From $\langle S_z\rangle$ we see that the centers are only partially magnetized. Bottom: the laser pulse envelope. See also Table V.

From the above mentioned discussions we summarize that global spin control on each dimer is possible with triplet excited states due to unequal distribution of spin densities on each dimer, with the inclusion of quintets in the excited the distribution of spin densities of each magnetic center becomes equal and this results to global spin switch scenarios within 600 fs. Moreover, we introduce an *irreversible* global demagnetization scenario within spin states originating from a single quintet set. All observed effects and scenarios are the immediate consequence of the delicate interplay of the two, three, or four magnetic centers of our structures, and the derived global or local functionalities evidently lie in their cooperative effects.

IV. CONCLUSIONS

In this manuscript we systematically increase the number of magnetic centers from the two-magnetic-center cluster Ni_2 first to the three-magnetic-center cluster Ni_3Na_2, and then to the four-magnetic-center double nickel dimer $(Ni_2)_2$. We also increase the multiplicities (from singlets and triplets up to the inclusion of quintets). Our main findings are as follows.

(a) In the two-magnetic-center nickel cluster Ni_2: (i) high fidelity global spin switch is possible within 900 fs. (ii) Spin switching is also possible by the M process, where more intermediate states take part with substantially high occupations.

(b) In the three-magnetic-center cluster Ni_3Na_2: (i) functional cooperativity effect such as simultaneous spin flip and spin transfer (spin switch transfer) is possible with a high intense laser pulse and longer transition time. Such processes are possible when state interlocking occurs. (ii) Laser-induced ultrafast local spin switches and spin transfers are possible within transition time of 600 fs and 300 fs. (iii) With the inclusion of quintets we find local-spin flips on individual Ni atoms and also observe a highly nonlinear M process, closely related to the M process in Ni_2. (iv) Ultrafast local demagnetization scenarios can be achieved within 500–600 fs.

(c) In the four-magnetic-center double dimer $(Ni_2)_2$: (i) Spin control on each dimer is possible only with the triplets in the excited states. (ii) Global magnetization dynamics is possible with the inclusion of quintets states. (iii) Inclusion of higher multiplicities results in an irreversible global demagnetization process. (iv) All spin-manipulation scenarios take place within 600 fs. As a general conclusion we may state that the systematically studied, coherent spin control on multimagnetic-center molecular structures opens an avenue for designing logic elements and spintronic devices.

ACKNOWLEDGMENTS

The authors acknowledge funding from the German Research Foundation (DFG) via the Transregional Collaborative Research Center SFB/TRR 88 “3MET”. D.C. and H.P.X. contributed equally to this manuscript.

[1] E. Beaurepaire, J.-C. Merle, A. Daunois, and J.-Y. Bigot, Phys. Rev. Lett. **76**, 4250 (1996).

[2] J. Hohlfeld, E. Matthias, R. Knorren, and K. H. Bennemann, Phys. Rev. Lett. **78**, 4861 (1997).

[3] A. Scholl, L. Baumgarten, R. Jacquemin, and W. Eberhardt, Phys. Rev. Lett. **79**, 5146 (1997).

[4] B. Koopmans, M. van Kampen, J. T. Kohlhepp, and W. J. M. de Jonge, Phys. Rev. Lett. **85**, 844 (2000).

[5] M. Vomir, L. H. F. Andrade, L. Guidoni, E. Beaurepaire, and J.-Y. Bigot, Phys. Rev. Lett. **94**, 237601 (2005).

[6] G. Lefkidis, G. P. Zhang, and W. Hübner, Phys. Rev. Lett. **103**, 217401 (2009).

[7] J. M. Shaw, S. E. Russek, T. Thomson, M. J. Donahue, B. D. Terris, O. Hellwig, E. Dobisz, and M. L. Schneider, Phys. Rev. B **78**, 024414 (2008).

[8] J. M. Shaw, T. J. Silva, M. L. Schneider, and R. D. McMichael, Phys. Rev. B **79**, 184404 (2009).

[9] R. Gómez-Abal, O. Ney, K. Satitkovitchai, and W. Hübner, Phys. Rev. Lett. **92**, 227402 (2004).

[10] G. Lefkidis and W. Hübner, Phys. Rev. B **76**, 014418 (2007).

[11] A. Wolf and H.-H. Schmidtke, Int. J. Quantum Chem. **18**, 1187 (1980).

[12] U. Atxitia and O. Chubykalo-Fesenko, Phys. Rev. B **84**, 144414 (2011).

[13] G. P. Zhang and W. Hübner, Phys. Rev. Lett. **85**, 3025 (2000).

[14] K. Carva, M. Battiato, and P. M. Oppeneer, Phys. Rev. Lett. **107**, 207201 (2011).

[15] M. Moskovits and J. E. Hulse, J. Chem. Phys. **66**, 3988 (1977).

[16] M. Rasanen, L. A. Heimbrook, and V. E. Bondybey, J. Mol. Struct. **157**, 129 (1987).

[17] M. Krauß, T. Roth, S. Alebrand, D. Steil, M. Cinchetti, M. Aeschlimann, and H. C. Schneider, Phys. Rev. B **80**, 180407 (2009).

[18] C. Stamm, N. Pontius, T. Kachel, M. Wietstruk, and H. A. Dürr, Phys. Rev. B **81**, 104425 (2010).

[19] T. Roth, A. J. Schellekens, S. Alebrand, O. Schmitt, D. Steil, B. Koopmans, M. Cinchetti, and M. Aeschlimann, Phys. Rev. X **2**, 021006 (2012).

[20] M. Battiato, K. Carva, and P. M. Oppeneer, Phys. Rev. Lett. **105**, 027203 (2010).

[21] B. Koopmans, J. J. M. Ruigrok, F. Dalla Longa, and W. J. M. de Jonge, Phys. Rev. Lett. **95**, 267207 (2005).

[22] J.-Y. Bigot, M. Vomir, and E. Beaurepaire, Nat. Phys. **5**, 515 (2009).

[23] N. Kazantseva, U. Nowak, R. W. Chantrell, J. Hohlfeld, and A. Rebei, Europhys. Lett. **81**, 27004 (2008).

[24] U. Atxitia, O. Chubykalo-Fesenko, N. Kazantseva, D. Hinzke, U. Nowak, and R. W. Chantrell, Appl. Phys. Lett. **91**, 232507 (2007).

[25] U. Atxitia, O. Chubykalo-Fesenko, J. Walowski, A. Mann, and M. Münzenberg, Phys. Rev. B **81**, 174401 (2010).

[26] T. Hartenstein, G. Lefkidis, W. Hübner, G. P. Zhang, and Y. Bai, J. Appl. Phys. **105**, 07D305 (2009).

[27] W. Hübner, S. Kersten, and G. Lefkidis, Phys. Rev. B **79**, 184431 (2009).

[28] C. Li, T. Hartenstein, G. Lefkidis, and W. Hübner, Phys. Rev. B **79**, 180413 (2009).

[29] J. Schnack, M. Brüger, M. Luban, P. Kögerler, E. Morosan, R. Fuchs, R. Modler, H. Nojiri, R. C. Rai, J. Cao *et al.*, Phys. Rev. B **73**, 094401 (2006).

[30] K. Iida, S.-H. Lee, T. Onimaru, K. Matsubayashi, and T. J. Sato, Phys. Rev. B **86**, 064422 (2012).

[31] W. Jin, M. Becherer, D. Bellaire, G. Lefkidis, M. Gerhards, and W. Hübner, Phys. Rev. B **89**, 144409 (2014).

[32] W. Jin, F. Rupp, K. Chevalier, M. M. N. Wolf, M. C. Rojas, G. Lefkidis, H.-J. Krüger, R. Diller, and W. Hübner, Phys. Rev. Lett. **109**, 267209 (2012).

[33] G. Pal, G. Lefkidis, and W. Hübner, J. Phys. Chem. A **113**, 12071 (2009).

[34] In Fig. 3 the role of these states are played by triplets $|4\rangle$: $|A\rangle$, $|47\rangle$: $|B\rangle$, a mixture of $|16\rangle$ and $|17\rangle$: $|C\rangle$, $|48\rangle$: $|D\rangle$, and $|E\rangle$: $|5\rangle$.

[35] V. Chaltykyan, E. Gazazyan, G. Grigoryan, A. Hovhannisyan, and O. Tikhova, J. Phys. Conf. Ser. **350**, 012004 (2012).

[36] S. Ghosh, J. Opt. Soc. Am. B **30**, 2540 (2013).

[37] K. Bergmann, H. Theuer, and B. W. Shore, Rev. Mod. Phys. **70**, 1003 (1998).

[38] M. J. Frisch, G. W. Trucks, H. B. Schlegel, G. E. Scuseria, M. A. Robb, J. R. Cheeseman, G. Scalmani, V. Barone, B. Mennucci, G. A. Petersson *et al.*, *Gaussian09 Revision D.01* (Gaussian Inc., Wallingford, CT, 2009).

[39] H. Koch, H. J. A. Jensen, P. Jørgensen, and T. Helgaker, J. Chem. Phys. **93**, 3345 (1990).

[40] J. F. Stanton and R. J. Bartlett, J. Chem. Phys. **98**, 7029 (1993).

[41] M. Kállay and J. Gauss, J. Chem. Phys. **121**, 9257 (2004).

[42] A. Krylov, Rev. Phys. Chem. **59**, 433 (2008).

[43] S. V. Levchenko, Ph.D. thesis, University of Southern California, 2005.

[44] A. I. Krylov, Chem. Phys. Lett. **338**, 375 (2001).

[45] H. Nakatsuji, M. Hada, M. Ehara, K. Toyota, J. Fukuda, R. Hasegawa, M. Ishida, T. Nakajima, Y. Honda, O. Kitao, and H. Nakai, http://www.sbchem.kyoto-u.ac.jp.

[46] L. Meissner and R. J. Bartlett, J. Chem. Phys. **94**, 6670 (1991).

[47] M. Nooijen, K. R. Shamasundar, and D. Mukherjee, Mol. Phys. **103**, 2277 (2005).

[48] J. F. Stanton, J. Chem. Phys. **101**, 8928 (1994).

[49] H. Xiang, G. Lefkidis, and W. Hübner, Phys. Rev. B **86**, 134402 (2012).

[50] D. Chaudhuri, G. Lefkidis, A. Kubas, K. Fink, and W. Hübner, in *Proceedings of the International Conference UMC 2013 Strasbourg, France*, Springer Proceedings in Physics Vol. 159 (Springer, New York, 2013), pp. 159–161.

[51] W. Jin, Ph.D. thesis, University of Kaiserslautern, 2013.

[52] G. P. Zhang, G. Lefkidis, W. Hübner, and Y. Bai, J. Appl. Phys. **109**, 07D303 (2011).

[53] H. Nakatsuji and K. Hirao, J. Chem. Phys. **68**, 2053 (1970).

[54] S. Koseki, M. W. Schmidt, and M. S. Gordon, J. Phys. Chem. A **102**, 10430 (1998).

[55] G. Lefkidis and W. Hübner, Phys. Rev. B **74**, 155106 (2006).

[56] T. Hartenstein, C. Li, G. Lefkidis, and W. Hübner, J. Phys. D **41**, 164006 (2008).

[57] H. Xiang, G. Lefkidis, and W. Hübner, J. Supercond. Nov. Magn. **26**, 2001 (2013).

[58] C. Li, S. Zhang, W. Jin, G. Lefkidis, and W. Hübner, Phys. Rev. B **89**, 184404 (2014).

[59] W. Jin, C. Li, G. Lefkidis, and W. Hübner, Phys. Rev. B **89**, 024419 (2014).

[60] G. Lefkidis and W. Hübner, J. Magn. Magn. Mater. **321**, 979 (2009).
[61] R. R. Cash and A. H. Karp, ACM Trans. Math. Softw. **16**, 201 (1990).
[62] W. R. Wadt and P. J. Hay, J. Chem. Phys. **82**, 284 (1985).
[63] P. J. Hay and W. R. Wadt, J. Chem. Phys. **82**, 299 (1985).
[64] R. Gómez-Abal and W. Hübner, Phys. Rev. B **65**, 195114 (2002).
[65] Y. Wu, E. D. Kim, X. Xu, J. Cheng, D. G. Steel, A. S. Bracker, D. Gammon, S. E. Economou, and L. J. Sham, Phys. Rev. Lett. **99**, 097402 (2007).
[66] G. Lefkidis, C. Li, G. Pal, M. Blug, H. Kelm, H.-J. Krüger, and W. Hübner, J. Phys. Chem. A **115**, 1774 (2011).
[67] J. P. Gauyacq and N. Lorente, Phys. Rev. B **87**, 195402 (2013).